photonics

MDPI

Article

Utilizing States of Polarization in One-Dimensional Corite Codes with Two-Code Keying for Optical Code-Division Multiple Access

Bih-Chyun Yeh

Department of Electrical Engineering, Chang Gung University, Taoyuan City 33302, Taiwan; bih.chyun.yeh@gmail.com

Abstract: We propose a novel family of codes comprising two mutually orthogonal states of polarization (SOPs) for the spectral encoding of one-dimensional (1D) Corite codes with two-code keying (TCK) for use in the spectral amplitude coding (SAC) of optical code-division multiple access (OCDMA) networks. We design these 1D Corite codes with TCK to create a specific code operation function, an encoding optical transmitter structure, and a decoding optical receiver structure, respectively. In the proposed system, multi-user interference (MUI) can occur due to interference from other simultaneous users. However, we have modified the cross-correlation to cancel out the MUI. Although the proposed system recovers bits successfully, it still suffers from phase-induced intensity noise (PIIN). Our numerical results demonstrate that the proposed system using 1D Corite codes with TCK can support a larger number of simultaneous users than other systems that use 1D CTP codes with TCK, 1D M3 sequence codes, 1D BIBD codes, and 1D BDS codes with TCK. Specifically, the proposed system can support up to 48 simultaneous users, which is a notable improvement. Our numerical results indicate that the proposed system using 1D Corite codes with TCK can achieve a data transmission rate of up to 2.5 Gbps, which is a significant improvement.

Keywords: multi-user interference (MUI); optical polarization (OP); optical code-division multiplexing (OCDMA); two-code keying (TCK)

Citation: Yeh, B.-C. Utilizing States of Polarization in One-Dimensional Corite Codes with Two-Code Keying for Optical Code-Division Multiple Access. *Photonics* **2024**, *11*, 819. https://doi.org/10.3390/photonics11090819

Received: 28 June 2024
Revised: 28 August 2024
Accepted: 29 August 2024
Published: 30 August 2024

1. Introduction

The code sequences used in the OCDMA system [1–8] exhibit cross-correlation values, making them suitable for spread-spectrum communication environments. Numerous research papers have explored different code families to develop optical code-division multiple access (OCDMA) systems. The spectral amplitude coding (SAC) scheme [9–12] was a popular technique for implementing OCDMA networks due to its ability to mitigate multi-user interference (MUI). This scheme required the creation of a cross-correlation value and balanced photodetectors [13–20] matched to the decoded signals. However, SAC schemes suffered from phase-induced intensity noise (PIIN) due to optical noise. According to complementary keying modulation (CKM), cross-correlation values [21,22] could limit network performance. Code sequences were designed to incorporate compact SACs into transmitters and receivers. However, detecting the differential output of the received signals required an installation on each receiver. In long-distance transmissions using optical fiber, the signals were severely affected, which further underscored the importance of optimizing the code sequences used in the OCDMA system.

H. Chen et al. [23] proposed a tunable encoder/decoder for spectrum amplitude coding in optical code-division multiple access (SAC-OCDMA) passive optical networks based on the polarization modulation of liquid crystal (LC) materials. The encoder/decoder was constructed using LC materials with a blocking ratio for unwanted spectral slices. It had the added advantage of having a flexible reconfiguration for the coded addresses. The processor was eventually used as an encoder and decoder for the SAC-OCDMA

system. In their experiment, the researchers demonstrated the algorithm's coding and decoding performance for the first time. Using an encoder/decoder with a blocking ratio, the experimental results proved that it suppressed unwanted spectral slices. In addition, it was efficient at encoding and decoding. The experiment verified that the blocking ratio was more than 40 dB. This resulted in the creation of an encoder/decoder for the SAC-OCDMA PON.

N. G. Tarhuni [24] developed the OCDMA to address multiple-beam interference, which was a common problem in optical networks. The OCDMA offered a promising solution for efficiently sharing resources in such networks. The OCDMA's effect on an optical network was analyzed by encoding the state of polarization (SOP). In this approach, the SOP of each node was rotated based on signature codes. The signature codes included the asynchronous Gold code set and the synchronous Hadamard code set. The system performance was analyzed based on the signal-to-noise ratio (SNR) and the bit error rate (BER). While the performance was satisfactory for single-node transmission, it degraded as more nodes were transmitted concurrently on the shared channel. However, when the synchronous Hadamard code set was used as the signature waveform, the system's BER performance improved as the number of active nodes increased. J. P. Heritage et al. [25] employed polarization multiplexing to generate a six-user data stream, which experienced polarization dispersion issues. This problem was more significant than the noise introduced by polarization dispersion.

We propose an innovative set of 1D Corite codes with two-code keying (TCK) for the OCDMA system with the intention of improving its performance through the use of a set of two mutually orthogonal states of polarization (SOPs). With more concurrent users accessing the set of two mutually orthogonal SOPs simultaneously, novel behavior is observed, leading to an improved performance. Furthermore, the 1D Corite codes with TCK using the proposed system are validated under various conditions. The presence of multi-user interference (MUI) can degrade the BER performance of the OCDMA system; however, our proposed system creates a modified cross-correlation to eliminate MUI and suppress PIIN in terms of performance. In addition, we propose using 1D Corite codes with TCK to achieve a better performance. According to the numerical results, the performance of the proposed system using the 1D Corite codes with TCK is better when using 48 simultaneous users, a data transmission rate of 2.5 Gbps, and an effective source power of -12dBm, in comparison to that of other systems that use 1D CTP codes with TCK [26], 1D M3 sequence codes [27], 1D BIBD codes [28], and 1D BDS codes with TCK [29].

This paper is structured as follows: Section 2 explains the development of polarization and modified cross-correlation to design 1D Corite codes with TCK. Section 3 discusses the proposed structure of the 1D Corite codes with TCK in the polarization and SAC-OCDMA systems. Section 4 focuses on the analysis of the equations used in the 1D Corite codes with TCK in the polarization and SAC-OCDMA systems. The numerical results are presented and discussed in Section 5. Section 6 is the discussion. Finally, the conclusions drawn from the simulation are summarized in Section 7.

2. One-Dimensional Corite Codes with TCK

We propose the use of 1D Corite codes for OCDMA based on a novel family of SAC-OCDMA systems with novel codes. One-dimensional Corite codes are constructed using a number sequence $\delta_{\alpha,\beta}$, which enhances their generation. The proposed structure for building optical transmitters, a polarization-maintaining star coupler (PMSC), and optical receivers includes code sequences of the 1D Corite codes. A PMSC is a polarization-maintaining star coupler, which ensures polarization retention and stability. The cross-correlation of 1D Corite codes results in non-zero values or zero values. The code sequences of the 1D Corite codes employ two-polarization spectral encoding schemes to complete the proposed system.

The parameters of ξN, ξ, and Ω can be used to classify 1D Corite codes, where ξN represents the code length, ξ represents the code weight, and Ω represents cross-correlation.

The cross-correlation theorem is used to estimate multiplication and addition operations, generating a matrix with non-zero or zero values. The number sequence determines the code weight, code length, and code size. This number sequence $\delta_{\alpha,\beta}$ produces the newly developed family of 1D Corite codes. The Galois field GF (ξ) uses prime fields for each prime number ξ to establish arithmetic rules. In this case, the function GF (ξ) can only be generated by the primitive irreducible polynomial. The number sequence $\delta_{\alpha,\beta}$ contains elements of GF (ξ) and is formulated as follows:

$$\delta_{\alpha,\beta} = ((\beta + 1) * (N - 1) + (\alpha + \gamma)) + 1, \tag{1}$$

where the values of $\delta_{\alpha,\beta}$ are integers with integer number α, integer number β, and integer number γ. We develop the 1D Corite codes with TCK by having (β+1), (N−1), and (α+γ) cooperate through multiplication and addition. Hence, the term "cooperate" corresponds to the creation of the 1D Corite codes with TCK. The symbols $*$, $+$, and $-$ denote the modulo of the multiplication, addition, and subtraction operations, respectively. The integer number α ranges from 0 to $N - 1$, integer number β ranges from 0 to $\xi - 1$, and integer number γ ranges from 0 to $N - 1$. Each number sequence $\delta_{\alpha,\beta}$ has a unique pattern determined by the parameters α, β, N, and γ. The parameters α, β, N, and γ use the operations to find the modulo operator according to modular arithmetic. The modulo addition operates on β and 1 and on α and γ. The modulo subtraction operates on N and 1. The modulo multiplication operates on (β+1) and (N−1), the modulo addition operates on (β+1)$*$(N−1), and (α+γ), and the modulo addition operates on (β+1)$*$(N−1)+(α+γ), and 1. By using the number sequence $\delta_{\alpha,\beta}$, we can perform algebraic operations on integer numbers. The value of the number sequence $\delta_{\alpha,\beta}$ produces the code sequences of the 1D Corite codes. The proposed codes employ 1D Corite codes, and the number sequence $\delta_{\alpha,\beta}$ is used to generate the codes. Therefore, the newly developed family of codes for 1D Corite codes operates with the number sequence $\delta_{\alpha,\beta}$.

The code sequence $M(\alpha)$ is derived from the binary numbers $m_{\alpha,g}$, which are obtained from each generated number sequence $\delta_{\alpha,\beta}$. In other words, the codes are generated by taking the number sequence $\delta_{\alpha,\beta}$ from the binary number $m_{\alpha,g}$, which becomes code sequence $M(\alpha)$. The integer number α is used to obtain the binary number $m_{\alpha,g}$ as follows:

$$m_{\alpha,g} = \begin{cases} 1, & g = \delta_{\alpha.\beta} + \beta\xi, \\ 0, & otherwise, \end{cases} \tag{2}$$

where α = 0, 1, 2, …, $N - 1$, and g = 0, 1, …, $N\xi - 1$. The binary number $m_{\alpha,g}$ of the code sequence $M(\alpha)$ is obtained from the number sequence $\delta_{\alpha,\beta}$ through addition and multiplication operations to create an integer number g. The number sequences $\delta_{\alpha,\beta}$ with α = 0, 1, 2, …, $N - 1$ and β = 0, 1, 2, …, $\xi - 1$ are used to determine the integer value of the binary number $m_{\alpha,g}$ for the code sequence $M(\alpha)$. Equation (2) outlines this process. With the number sequence $\delta_{\alpha,\beta}$, we can create the binary number $m_{\alpha,g}$ for the corresponding code sequence $M(\alpha)$ in the 1D Corite codes. In 1D Corite codes, the code sequence is generated based on the number of simultaneous users and the code weight. Table 1 illustrates the 1D Corite codes for N = 10 and ξ = 2.

The 1D Corite codes utilize code sequences $M(\alpha)$ and $M(\alpha')$ to traverse two mutually orthogonal SOPs, where g = 0, …, $N\xi - 1$. Thus, the $m_{\alpha,g}$ and $m_{\alpha',g}$ in the components are associated with the two mutually orthogonal SOPs. The code sequences $M(\alpha)$ and $M(\alpha')$ can be expressed as follows:

$$M(\alpha) = [m_{\alpha,0}, m_{\alpha,1}, m_{\alpha,2}, \ldots, m_{\alpha,N\xi-1}], \tag{3}$$

$$M(\alpha') = [m_{\alpha',0}, m_{\alpha',1}, m_{\alpha',2}, \ldots, m_{\alpha',N\xi-1}], \tag{4}$$

where the code length $N\xi$ of the 1D Corite codes is obtained by multiplying N and prime number ξ. In the code sequence $M(\alpha)$, the value of α corresponds to the element of (3), while in the code sequence $M(\alpha')$, the value of α corresponds to the element of (4).

Table 1. One-dimensional Corite codes with code weight = 2 and code length = 20.

Code Sequences																			
0	0	0	0	0	0	0	1	0	0	0	0	0	0	0	0	1	0	0	0
0	0	0	0	0	0	0	0	1	0	0	0	0	0	0	0	0	1	0	0
0	0	0	0	0	0	0	0	0	1	0	0	0	0	0	0	0	0	1	0
1	0	0	0	0	0	0	0	0	0	0	0	0	0	0	0	0	0	0	1
0	1	0	0	0	0	0	0	0	0	1	0	0	0	0	0	0	0	0	0
0	0	1	0	0	0	0	0	0	0	0	1	0	0	0	0	0	0	0	0
0	0	0	1	0	0	0	0	0	0	0	0	1	0	0	0	0	0	0	0
0	0	0	0	1	0	0	0	0	0	0	0	0	1	0	0	0	0	0	0
0	0	0	0	0	1	0	0	0	0	0	0	0	0	1	0	0	0	0	0
0	0	0	0	0	0	1	0	0	0	0	0	0	0	0	1	0	0	0	0

The cross-correlation theorem specifies that sets of code sequences can be used to perform permutations of the code sequence. Permutations are represented by cross-correlation functions. In the context of 1D Corite codes, the cross-correlations $\Omega(\alpha, r)$ and $\Omega(\alpha', r')$ generate the code sequences $M(\alpha)$ and $M(r)$ and the code sequences $M(\alpha')$ and $M(r')$ in the following manner:

$$\Omega(\alpha, r) = \sum_{g=0}^{N\xi-1} m_{\alpha,g} m_{r,g}, \tag{5}$$

and

$$\Omega(\alpha', r') = \sum_{g=0}^{N\xi-1} m_{\alpha',g} m_{r',g}. \tag{6}$$

$\Omega(\alpha, r)$ corresponds to the (α, r)-th entry of $m_{\alpha,g}$ and $m_{r,g}$, while $\Omega(\alpha', r')$ corresponds to the (α', r')-th entry of $m_{\alpha',g}$ and $m_{r',g}$, where g takes on values from 0, 1, 2, …, $N\xi - 1$. The cross-correlations of $\Omega(\alpha, r)$ and $\Omega(\alpha', r')$ involve multiplying the code sequences $m_{\alpha,g}$, $m_{r,g}$ and $m_{\alpha',g}$, $m_{r',g}$ of the 1D Corite codes and summing the products $m_{\alpha,g}m_{r,g}$ and $m_{\alpha',g}m_{r',g}$. By performing cross-correlation operations on the 1D Corite codes, the proposed codes generate auto-correlation and cross-correlation results. The cross-correlations $\Omega(\alpha, r)$ for 0-degree polarization and $\Omega(\alpha', r')$ for 90-degree polarization can be expressed as follows:

$$\Omega(\alpha, r) = \begin{cases} \xi, & \alpha = r, \\ 0, & otherwise, \end{cases} \tag{7}$$

and

$$\Omega(\alpha', r') = \begin{cases} \xi, & \alpha' = r', \\ 0, & otherwise. \end{cases} \tag{8}$$

When $\alpha = r$ and $\alpha' = r'$, the cross-correlations $\Omega(\alpha, r)$ and $\Omega(\alpha', r')$ are equal to ξ. When $\alpha \neq r$ and $\alpha' \neq r'$, the cross-correlations $\Omega(\alpha, r)$ and $\Omega(\alpha', r')$ are equal to 0. Therefore, the cross-correlations of $\Omega(\alpha, r)$ and $\Omega(\alpha', r')$ combine the code sequence $M(\alpha)$ and $M(r)$ and the code sequence $M(\alpha')$ and $M(r')$ to perform the cross-correlation, resulting in $\Omega(\alpha, r)$ and $\Omega(\alpha', r')$ being ξ (when $\alpha = r$ or $\alpha' = r'$) or 0 (when $\alpha \neq r$ or $\alpha' \neq r'$). Thus, the cross-correlations $\Omega(\alpha, r)$ and $\Omega(\alpha', r')$ include auto-correlation when ξ (when $\alpha = r$ or $\alpha' = r'$) or the cross-correlations are 0 (when $\alpha \neq r$ or $\alpha' \neq r'$). The absence of MUI results in the auto-correlation values of ξ and $-\xi$, as well as a cross-correlation value of 0. The cross-correlations $\Omega(\alpha, r)$ and $\Omega(\alpha', r')$ result in no influence from multiple users, effectively eliminating MUI.

We specify the following to define the values of the modified cross-correlation between $\Omega(\alpha, r)$ and $\Omega(\alpha', r')$:

$$\Psi(\alpha, r, \alpha', r') = \Omega(\alpha, r) - \Omega(\alpha', r') = \begin{cases} \xi, & \alpha = r, \\ -\xi, & \alpha' = r', \\ 0, & otherwise. \end{cases} \tag{9}$$

We use the cross-correlations of $\Omega(\alpha, r)$ for 0-degree polarization and $\Omega(\alpha', r')$ for 90-degree polarization. If we assume that $\alpha = r$ with $\Omega(\alpha, r)$, the modified cross-correlation $\psi(\alpha, r, \alpha', r')$ will be equal to ξ according to (7). Similarly, if we assume that $\alpha' = r'$ with $\Omega(\alpha', r')$, the modified cross-correlation $\psi(\alpha, r, \alpha', r')$ will be equal to $-\xi$ as in (8). For all other cases, the modified cross-correlation $\psi(\alpha, r, \alpha', r')$ will be equal to 0 as in (9). By assigning the values of the modified cross-correlation $\psi(\alpha, r, \alpha', r')$ to be ξ, $-\xi$, or 0, we can determine the value of cross-correlations $\Omega(\alpha, r)$ and $\Omega(\alpha', r')$. The modified cross-correlation from 1D Corite codes with TCK utilizes cross-correlations to eliminate interferences from other simultaneous users, known as MUI. At the same time, we observe the modified cross-correlation $\Psi(\alpha, r, \alpha', r')$ to ensure the auto cross-correlation is ξ and $-\xi$, and the cross-correlation is 0, as the modified cross-correlation $\Psi(\alpha, r, \alpha', r')$ can remove MUI. The proposed codes enhance the modified cross-correlation $\psi(\alpha, r, \alpha', r')$ to eliminate interferences and achieve ideal cross-correlation. The proposed codes offer the modified cross-correlation $\psi(\alpha, r, \alpha', r')$ to eliminate interferences from 1D Corite codes with TCK.

3. System Description

In Figure 1, the proposed system involves 1D Corite codes with TCK that utilize two-polarization spectral encoding with all code sequences $M(\alpha)$, with ranges from $a = 0$, 1, 2, …, $N - 1$. The proposed system consists of N optical transmitters, an $N \times N$ PMSC, and N optical receivers. The PMSC employs a polarization-maintaining star coupler that ensures polarization retention and stability. Each optical transmitter is connected to the $N \times N$ PMSC, which acts as a connector to each optical receiver. The $N \times N$ PMSC provides the necessary connections to link the N optical transmitters and N optical receivers. The proposed system transmits optical light through N optical transmitters, an $N \times N$ PMSC, and N optical receivers. In the proposed system, the information bit is encoded into the code sequence of 1D Corite codes with TCK. It is transmitted through the N optical transmitters, sent through the $N \times N$ PMSC, and received by the N optical receivers. Each information bit uses two-polarization spectral encoding to design two-polarization spectral sequences of the 1D Corite codes with TCK in the optical transmitter. The $N \times N$ PMSC obtains all the code sequences of the 1D Corite codes and sends them to the N optical receiver.

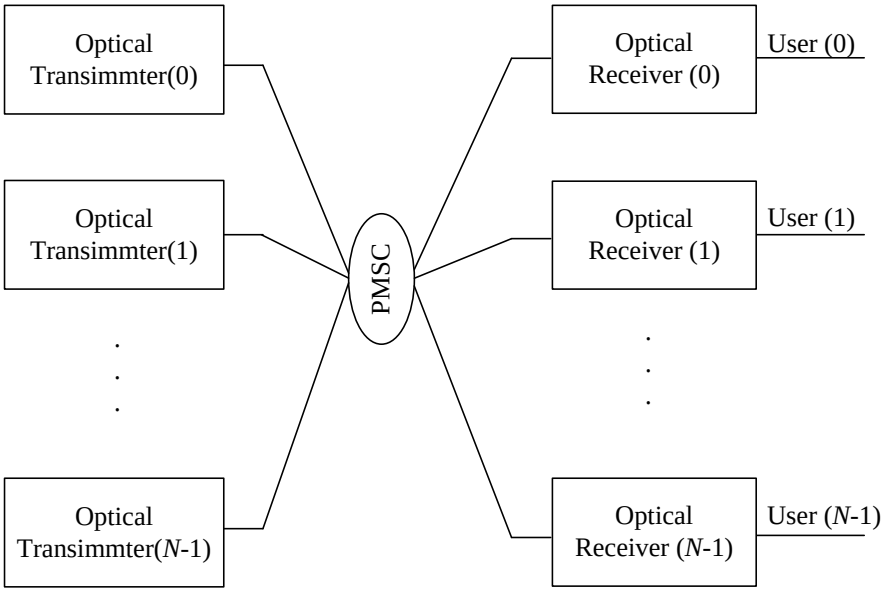

Figure 1. Schematic block diagram of 1D Corite codes with TCK.

The structure of the optical transmitter is shown in Figure 2, comprising several components such as a broadband light source (BLS), a polarizer, a polarization controller (PC), a polarization beam splitter (PBS), two electro-optic modulators (EOMs), two optical circulators, two fiber Brag gratings (FBGs), and polarization beam combiners (PBCs). The

BLS is connected to the polarizer, which is then connected to the polarization controller. The polarization controller utilizes the PBS to split the optical light into two polarizations, which are connected to the up EOM and down EOM. The up EOM and down EOM are linked to the up optical circulator and down optical circulator. Finally, the up and down optical circulators are connected to the up and down FBGs, which serve as the two polarizations of the PBC.

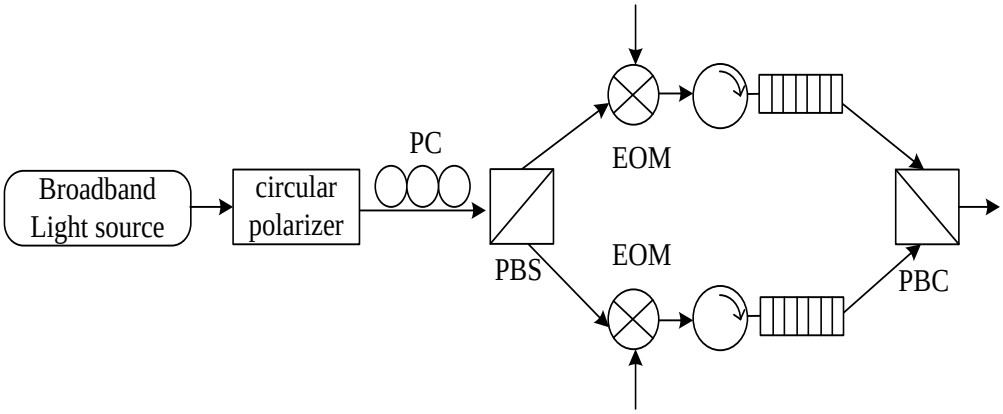

Figure 2. The structure of the optical transmitter.

The optical transmitter structure aims to generate two code sequences of the 1D Corite codes with TCK. The BLS transmits optical light, which is then passed through the polarizer. The polarizer produces two mutually orthogonal SOPs, such as vertical and horizontal orthogonal SOPs. The polarizer and PC are adjusted to create a power ratio of 1:1 for the two orthogonally polarized light beams. The PC uses two mutually orthogonal SOPs and PBS to split the optical light into two polarizations, which are sent through the up EOM and down EOM. Using the two mutually orthogonal SOPs, the up EOM and down EOM modulate the optical light to carry the information bits b_i and $\overline{b_i}$. The up optical circulator and down optical circulator send modulated signals through the up FBG and down FBG. The reversing paths of the up optical circulator and down optical circulator originate from the spectral components, which reflect the numbers of gratings with complementary code sequences in the up FBG and down FBG before exiting from them. The passing paths of the up optical circulator and down optical circulator traverse the spectral components to transmit the numbers of gratings acquired from the up FBG and down FBG. The routes taken by the optical signals traverse the PBC. The PBC takes in two code sequences and allocates them to two polarization-spectral encodings, producing the two-polarization code sequences of the 1D Corite codes with TCK.

As shown in Figure 3, the optical receiver structure comprises 1×2 PBS, two optical circulators, two FBGs, and two photodiodes. Inputting the 1×2 PBS obtains the two-polarization code sequences of the 1D Corite codes with TCK, which are converted into two polarizations of the 1×2 PBS, which correspond to the two code sequences of the 1D Corite codes with TCK. These two polarizations of the 1×2 PBS connect to two optical circulators, which transmit the two code sequences of the 1D Corite codes with TCK to two FBGs. Two numbers of gratings within the two FBGs correspond to two complementary code sequences of the 1D Corite codes with TCK. Two FBGs reflect two specific spectral components of two complementary code sequences of the 1D Corite codes with TCK back along the two distinct reverse paths. These two reverse paths, each utilizing two numbers of gratings corresponding to the two complementary code sequences of the two FBGs, are connected to two optical circulators that exit from them. The two FBGs act as filters for the two grating numbers, transforming them into two code sequences of the 1D Corite codes with TCK along two distinct passing paths, leading to the activation of two photodiodes. The 1×2 PBS input of the receiver obtains one optical signal in two polarizations. The 1×2 PBS separates one optical signal in two polarizations into two optical signals with

0-degree and 90-degree polarizations. The 0-degree polarization signal passes through the optical circulator, which directs it to the input FBG. The optical signal is reflected through the FBG, which contains gratings corresponding to the complementary code sequence, and passes through the code sequence $M(\alpha)$. The 90-degree polarization signal is directed to another FBG, which passes it through the code sequence $M(\alpha')$. Both optical signals are then directed to two photodiodes. The optical receiver acquires two-polarization code sequences of the 1D Corite codes with TCK, adjusting the two numbers of gratings with complementary code sequences from two FBGs. This process enables the generation of two photodiodes, each producing a recovered bit. The difference between photodiode PD0 and photodiode PD1 may yield a modified photocurrent, which is directly proportional to the modified cross-correlation.

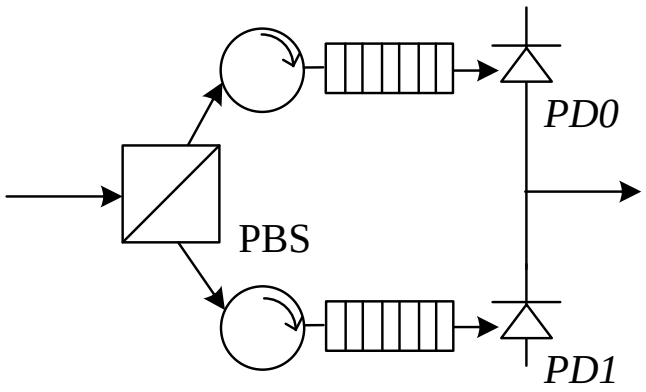

Figure 3. The structure of the optical receiver.

4. Performance Analysis

The photocurrents produced by the two photodiodes help to contain the photocurrent noises, which comprise the PIIN, shot noise, and thermal noise, which give rise to the currents, electron charge, and load resistance. The energy of the photocurrent noise results in variances in the photocurrent noise, resulting in statistically independent noise characteristics and contributing to PIIN variance, shot noise variance, and thermal noise variance. To achieve the BER, the performance analysis utilizes the modified photocurrent and photocurrent noise variances, including the PIIN variance, shot noise variance, and thermal noise variance. The BER estimation employs Gaussian approximation and calculates the photocurrent noise variances using the PIIN variance, shot noise variance, and thermal noise variance, as presented in [11,17].

$$\begin{aligned}\left\langle i^2_{noise,xbit}\right\rangle &= \left\langle i^2_{PIIN,xbit}\right\rangle + \left\langle i^2_{shot,xbit}\right\rangle + \left\langle i^2_{thermal,xbit}\right\rangle \\ &= B_r I^2_{PD,xbit}\tau_a + 2eI_{t,xbit}B_r + 4K_aT_nB_r/R_L.\end{aligned} \tag{10}$$

The photocurrent noise variances are based on various factors such as the modified photocurrent I_{PD}, coherence time of the incident light to the photodiode τ_a, total photocurrents I_t, electrical bandwidth B_r, electron charge e, Boltzmann's constant K_b, absolute noise temperature T_n, and load resistance R_L. To determine the PIIN, the shot noise and thermal noise are evaluated. Since photocurrent noises are statistically independent, each noise is considered separately. These noise variances are determined based on the PIIN variance, shot noise variance, and thermal noise variance, respectively.

The received optical signals generate the code sequences, resulting in a single-sideband power spectral density (PSD). To simplify the analysis, certain assumptions are made. Firstly, it is assumed that each spectrum component has the same spectral width. A broadband light source with a flat spectrum $[v_o - \Delta v/2, v_o + \Delta v/2]$ is assumed to have a center frequency and bandwidth of v_o and Δv, respectively. Additionally, when each

transmitter sends bits streams to each receiver, each receiver provides equal power to each user. For the analysis, the following definition is given for the g frequency division:

$$\Lambda(v,g) = \mathrm{K}\left[v - v_0 - \frac{\Delta v}{2\xi N}(-\xi N + 2g)\right] - \mathrm{K}\left[v - v_0 - \frac{\Delta v}{2\xi N}(-\xi N + 2g + 2)\right]. \quad (11)$$

The unit step function is defined by K(v) as follows:

$$\mathrm{K}(v) = \begin{cases} 1, & v \geq 0, \\ 0, & v < 0. \end{cases} \quad (12)$$

Based on these assumptions, the PSD of the received optical signals can be calculated as follows:

$$\Phi(v) = \frac{P_{sr}}{\Delta v} \sum_{y=1}^{Y} w(y) \sum_{g=0}^{\xi N-1} (m_{\alpha,g}) \Lambda(v,g). \quad (13)$$

The effective source power at the optical receiver is denoted by P_{sr}. The code weight is represented by ξ. The information bit of the w-th user, which is either "0" or "1", is given by $w(y)$. ξN is the code length of the spectral code sequence, while $m_{\alpha,g}$ defines an element of the codeword of the w-th user. In the worst-case scenario for interferences, $w(y)$ is set to "1" for $y = 1, 2, \ldots, N$. By employing the cross-correlation technique between codewords $m_{\alpha,g}m_{(y-1),g}$ and $m_{\alpha',g}m_{(y-1),g}$, we can ascertain the PD's resulting output currents from 0 using 0-degree polarization to 1 using 1-degree polarization. The expression for the output currents can be stated as follows:

$$\begin{aligned} I_{PD0,0bit} &= R\int_0^{\infty} \Phi_{0,0bit}(v)dv \\ &= R\frac{P_{sr}}{\Delta v}\int_0^{\infty} \sum_{y=1}^{Y} w(y) \sum_{g=0}^{\xi N-1} (m_{\alpha,g}m_{(y-1),g})\Lambda(v,g)dv \end{aligned} = R\frac{P_{sr}}{\xi N}[\xi], \quad (14)$$

$$\begin{aligned} I_{PD1,0bit} &= R\int_0^{\infty} \Phi_{1,0bit}(v)dv \\ &= R\frac{P_{sr}}{\Delta v}\int_0^{\infty} \sum_{y=1}^{Y} w(y) \sum_{g=0}^{\xi N-1} (m_{\alpha',g}m_{(y-1),g})\Lambda(v,g)dv \end{aligned} = 0, \quad (15)$$

or

$$\begin{aligned} I_{PD0,1bit} &= R\int_0^{\infty} \Phi_{0,1bit}(v)dv \\ &= R\frac{P_{sr}}{\Delta v}\int_0^{\infty} \sum_{y=1}^{Y} w(y) \sum_{g=0}^{\xi N-1} (m_{\alpha,g}m_{(y-1),g})\Lambda(v,g)dv \end{aligned} = 0, \quad (16)$$

$$\begin{aligned} I_{PD1,1bit} &= R\int_0^{\infty} \Phi_{1,1bit}(v)dv \\ &= R\frac{P_{sr}}{\Delta v}\int_0^{\infty} \sum_{y=1}^{Y} w(y) \sum_{g=0}^{\xi N-1} (m_{\alpha',g}m_{(y-1),g})\Lambda(v,g)dv \\ &= R\frac{P_{sr}}{\xi N}[\xi]. \end{aligned} \quad (17)$$

The photodiode's responsivity R is defined as $R = \eta e/hv_o$, where η is the quantum efficiency of the photodiode, e is the electron charge, h is Planck's constant, and v_o is the center frequency of the photodiode. The resulting photocurrent outputs of the total photodiode's *TPD* at the receiver can be expressed as follows:

$$\begin{aligned} I_{TPD,0bit} &= R\int_0^{\infty} [\Phi_{0,0bit}(v) - \Phi_{1,0bit}(v)]dv \\ &= [I_{PD0,0bit} - I_{PD1,0bit}] \\ &= R\frac{P_{sr}}{\xi N}\xi - 0, \\ &= R\frac{P_{sr}}{\xi N}\xi, \end{aligned} \quad (18)$$

or

$$\begin{aligned} I_{TPD,1bit} &= R\int_0^\infty [\Phi_{0,1bit}(v) - \Phi_{1,1bit}(v)]dv \\ &= [I_{PD0,1bit} - I_{PD1,1bit}] \\ &= 0 - R\frac{P_{sr}}{\xi N}\xi, \\ &= -R\frac{P_{sr}}{\xi N}\xi. \end{aligned} \tag{19}$$

We can use (20) to provide the *PIIN* variance. Based on the determination of the functions $\Phi_{0,xbit}(v)$ and $\Phi_{1,xbit}(v)$, $<i^2_{PIIN,xbit}>$ can be interpreted as follows:

$$\begin{aligned} \left\langle i^2_{PIIN,0bit} \right\rangle &= RB_r\int_0^\infty [\Phi_{0,0bit}(v) - \Phi_{1,0bit}(v)]^2 dv \\ = RB_r\int_0^\infty &\left[\Phi^2_{0,0bit}(v) + \Phi^2_{1,0bit}(v) - 2\Phi_{0,0bit}(v)\Phi_{1,0bit}(v)\right]dv \\ &= RB_r\int_0^\infty \left(\left[\Phi^2_{0,0bit}(v)\right] + \left[\Phi^2_{1,0bit}(v)\right]\right)dv. \end{aligned} \tag{20}$$

$2\Phi_{0,0bit}(v)\Phi_{1,0bit}(v)$ corresponds to zero because $\Phi_{0,0bit}(v)$ and $\Phi_{1,0bit}(v)$ have different signal components.

Or

$$\begin{aligned} \left\langle i^2_{PIIN,1bit} \right\rangle &= RB_r\int_0^\infty [\Phi_{0,1bit}(v) - \Phi_{1,1bit}(v)]^2 dv \\ = RB_r\int_0^\infty &\left[\Phi^2_{0,1bit}(v) + \Phi^2_{1,1bit}(v) - 2\Phi_{0,1bit}(v)\Phi_{1,1bit}(v)\right]dv \\ &= RB_r\int_0^\infty \left(\left[\Phi^2_{0,1bit}(v)\right] + \left[\Phi^2_{1,1bit}(v)\right]\right)dv. \end{aligned} \tag{21}$$

The equation is demonstrated by integrating the square of $\Phi_{0,xbit}(v)$ and $\Phi_{1,xbit}(v)$; the results are shown below.

$$\begin{aligned} &\int_0^\infty \Phi^2_{0,0bit}(v)dv \\ &= \frac{P^2_{sr}}{\Delta v^2}\int_0^\infty \left[\sum_{y=1}^{Y} w(y)\sum_{g=0}^{\xi N-1}(m_{\alpha,g}m_{(y-1),g})\Lambda(v,g)\right]^2 dv \ = \frac{P^2_{sr}}{\Delta v\xi N}[\xi], \end{aligned} \tag{22}$$

$$\begin{aligned} &\int_0^\infty \Phi^2_{1,0bit}(v)dv \\ &= \frac{P^2_{sr}}{\Delta v^2}\int_0^\infty \left[\sum_{y=1}^{Y} w(y)\sum_{g=0}^{\xi N-1}(m_{\alpha',g}m_{(y-1),g})\Lambda(v,g)\right]^2 dv \\ &= 0, \end{aligned} \tag{23}$$

or

$$\begin{aligned} &\int_0^\infty \Phi^2_{0,1bit}(v)dv \\ &= \frac{P^2_{sr}}{\Delta v^2}\int_0^\infty \left[\sum_{y=1}^{Y} w(y)\sum_{g=0}^{\xi N-1}(m_{\alpha,g}m_{(y-1),g})\Lambda(v,g)\right]^2 dv \\ &= 0, \end{aligned} \tag{24}$$

$$\begin{aligned} &\int_0^\infty \Phi^2_{1,1bit}(v)dv \\ &= \frac{P^2_{sr}}{\Delta v^2}\int_0^\infty \left[\sum_{y=1}^{Y} w(y)\sum_{g=0}^{\xi N-1}(m_{\alpha',g}m_{(y-1),g})\Lambda(v,g)\right]^2 dv \\ &= \frac{P^2_{sr}}{\Delta v\xi N}[\xi]. \end{aligned} \tag{25}$$

Assuming that every user has an equal probability of sending "0" or "1", (26) can be modified as follows:

$$\begin{aligned} \left\langle i^2_{PIIN,0bit} \right\rangle &= RB_r\left[\int_0^\infty \Phi^2_{0,0bit}(v)dv + \int_0^\infty \Phi^2_{1,0bit}(v)dv\right] \\ &= \frac{RB_rP^2_{sr}}{\Delta v\xi N}[\xi], \end{aligned} \tag{26}$$

or

$$\left\langle i^2_{PIIN,1bit} \right\rangle = RB_r \left[\int_0^\infty \Phi^2_{0,1bit}(v)dv + \int_0^\infty \Phi^2_{1,1bit}(v)dv \right] = \frac{RB_r P^2_{sr}}{\Delta v \xi N}[\xi]. \quad (27)$$

The PIIN variance has the most significant influence. Since ξ is the code weight and ξN is the code length, the PIIN variance is affected by both ξ and ξN. Therefore, when the influence of the PIIN is determined by the code weight and code length, the influence of the code weight divided by the code length results in the PIIN variance. Consequently, the influence of the PIIN leads to a loss in SNR.

The shot noise arises from the electron's charge and contributes to the random noise, which affects the shot noise variance. Assuming that the shot noise, PIIN, and thermal noise are mutually independent, we can obtain the shot noise variance. The shot noise also exhibits the shot noise variance, which can be demonstrated using the following expression:

$$\left\langle i^2_{shot,0bit} \right\rangle = 2eB_r[I_{PD0,0bit} + I_{PD1,0bit}], \quad (28)$$

or

$$\left\langle i^2_{shot,1bit} \right\rangle = 2eB_r[I_{PD0,1bit} + I_{PD1,1bit}]. \quad (29)$$

By substituting (14), (15) or (16), (17) into (28) or (29) and assuming an equal probability of "1" and "0" for every user, we obtain the shot noise variance as follows:

$$\left\langle i^2_{shot,0bit} \right\rangle = 2eB_r R \frac{P_{sr}}{\xi N}\xi, \quad (30)$$

or

$$\left\langle i^2_{shot,1bit} \right\rangle = 2eB_r R \frac{P_{sr}}{\xi N}\xi. \quad (31)$$

The shot noise variance prevents additional influence between $I_{PD0,0bit}$ and $I_{PD1,0bit}$ or $I_{PD0,1bit}$ and $I_{PD1,1bit}$. However, it does affect $I_{PD0,0bit}$ and $I_{PD1,0bit}$ or $I_{PD0,1bit}$ and $I_{PD1,1bit}$, causing their influence to increase. The SNR impacts the shot noise variance.

We attribute the thermal noise to the absolute noise temperature T_n, electrical bandwidth B_r, and load resistance R_L. Consequently, we can express the thermal noise variance as follows:

$$\left\langle i^2_{thermal,0bit} \right\rangle = \frac{4K_b T_n B_r}{R_L}, \quad (32)$$

or

$$\left\langle i^2_{thermal,1bit} \right\rangle = \frac{4K_b T_n B_r}{R_L}. \quad (33)$$

The thermal noise incorporates the absolute noise temperature T_n, electrical bandwidth B_r, and load resistance R_L. It utilizes these factors to increase the multiplication and division operations, which contributes to the influence. The SNR reflects this influence.

The algorithm generates $I^2_{TPD,0bit}$ or $I^2_{TPD,1bit}$ to produce the signal energies for SNR_{0bit} or SNR_{1bit}. SNR_{xbit} indicates the ratio of the signal energy to the noise energy based on the received signal. SNR_{0bit} or SNR_{1bit} can be determined by calculating $I^2_{TPD,0bit}$ using (18), (26), (30), and (32) or $I^2_{TPD,1bit}$ using (19), (27), (31), and (33), as expressed in (34). The noise energy is from the photocurrent noise variance. Depending on whether the transmitter uses 0 bits or 1 bit, the receiver operates with SNR_{0bit} or SNR_{1bit}, respectively. As such, the BER can be estimated as a function of the SNR given by [29]:

$$BER = \frac{erfc\left(\sqrt{(SNR_{0bit} or SNR_{1bit})/2}\right)}{2}. \quad (34)$$

It is therefore unsurprising that the BER can provide the performance of 1D Corite codes with TCK in terms of achieving the number of simultaneous users, data transmission rate, and effective source power.

5. Numerical Results

Three important parameters are used to evaluate the performance of the proposed system which uses 1D Corite codes with TCK, including the number of simultaneous users, data transmission rate, and effective source power. The performance is evaluated based on four plots: the BER versus the number of simultaneous users, the BER versus the data transmission rate, the BER versus the effective source power, and the spectral efficiency (SE) versus code length. During the simulation using the PIIN, the thermal noise and shot noise are considered to be the main sources of noise. Additionally, the PIIN is considered perturbative energy due to the modified cross-correlation property of the code sequences of the 1D Corite codes with TCK. To compare the performance of the 1D Corite codes with TCK, 1D CTP codes with TCK, 1D M3 sequence codes, 1D BIBD codes, and 1D BDS codes with TCK, modified cross-correlations are used, and MUI is removed. The numerical calculations are based on various parameters, including a PD quantum efficiency of $\eta = 0.6$, a receiver noise temperature of $T_n = 300$ K, a receiver load resistor of $R_L = 1030\ \Omega$, and a center wavelength $\lambda_o = 1550$ nm. The performance analysis is based on the numerical results using the 1D Corite codes with TCK, 1D CTP codes with TCK, 1D M3 sequence codes, 1D BIBD codes, and 1D BDS codes with TCK.

In Figure 4a, the SNR for the proposed 1D Corite codes with TCK is 18.46 dBm for 48 simultaneous users. For the 1D CTP codes with TCK, the SNR is 8.21 dBm with 48 simultaneous users. The 1D M3 sequence codes have an SNR of 12.82dBm with 48 simultaneous users. The 1D BIBD codes exhibit an SNR of 2.22 dBm with 48 simultaneous users, while the 1D BDS codes with TCK show an SNR of 6.77dBm with 48 simultaneous users. The SNR of the proposed system using 1D Corite codes with TCK surpasses that of systems using 1D CTP codes with TCK, 1D M3 sequence codes, 1D BIBD codes, and 1D BDS codes with TCK. Thus, the 1D Corite codes with TCK offer a better SNR performance compared to these other systems.

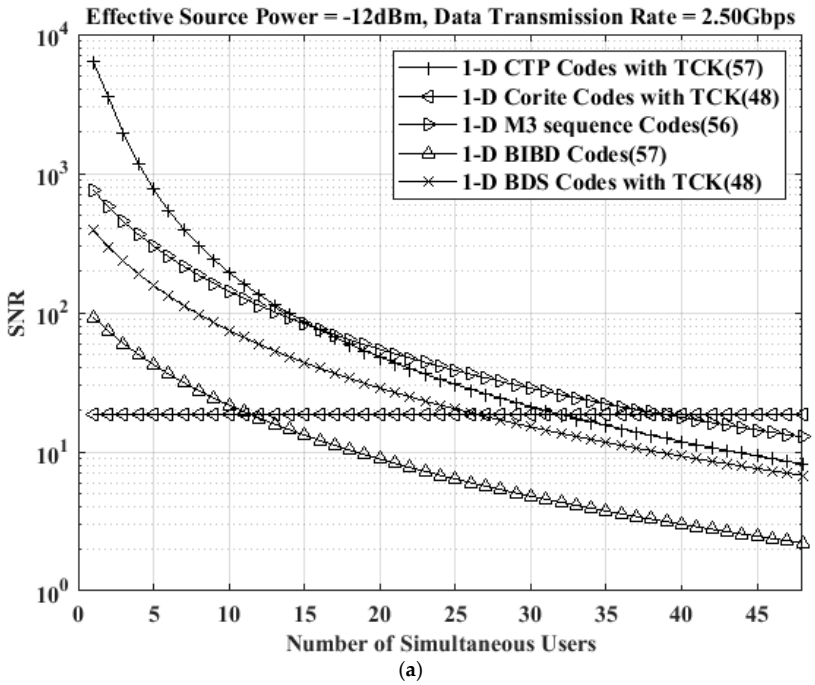

Figure 4. *Cont.*

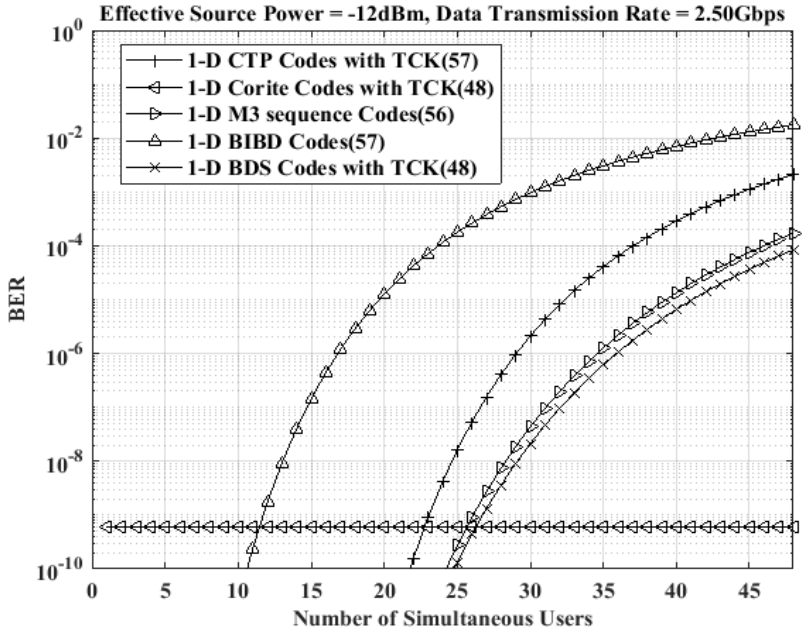

Figure 4. (**a**) Comparison of SNR in the proposed 1D Corite codes with TCK and other codes with different numbers of simultaneous users. (**b**) Comparison of BER in the proposed 1D Corite codes with TCK and other codes with different numbers of simultaneous users.

Figure 4b displays the impact of the number of simultaneous users on the BER in an OCDMA system that employs 1D Corite codes with TCK, 1D CTP codes with TCK, 1D M3 sequence codes, 1D BIBD codes, and 1D BDS codes with TCK. This is with a data transmission rate and effective source power of 2.5 Gbps and −12 dBm, respectively. The figure utilizes three type code sequences using the 1D Corite codes with TCK, 1D CTP codes with TCK, 1D M3 sequence codes, 1D BIBD codes, and 1D BDS codes with TCK to allow for simultaneous users, respectively. The evaluation the performance of the 1D Corite codes with TCK, 1D CTP codes with TCK, 1D M3 sequence codes, 1D BIBD codes, and 1D BDS codes with TCK indicates that the improvement for the 1D Corite codes with TCK is greater compared to that for the 1D CTP codes with TCK, 1D M3 sequence codes, 1D BIBD codes, and 1D BDS codes with TCK. The numerical results demonstrate that the proposed system based on 1D Corite codes with TCK outperforms conventional OCDMA systems that use 1D CTP codes with TCK, 1D M3 sequence codes, 1D BIBD codes, and 1D BDS codes with TCK. The OCDMA operation, which employs two polarizations for each user, enables a number of simultaneous users and their contributions. The complexity in 1D Corite codes with TCK is calculated as (the number of simultaneous users at the BER = 10^{-9}/total number of simultaneous users) * 100%. While other systems using 1D CTP codes with TCK, 1D M3 sequence codes, 1D BIBD codes, and 1D BDS codes with TCK can accommodate up to 23 (a complexity of 40.35%), 26 (a complexity of 46.43%), 11 (a complexity of 19.30%), and 27 (a complexity of 56.25%) simultaneous users, respectively, the proposed system using 1D Corite codes with TCK can handle up to 48 (a complexity of 100%) simultaneous users, with a BER of 10^{-9}. Therefore, the proposed system based on 1D Corite codes with TCK outperforms the other systems based on the 1D CTP codes with TCK, 1D M3 sequence codes, 1D BIBD codes, and 1D BDS codes with TCK, respectively. The proposed system using 1D Corite codes with TCK takes advantage of the modified cross-correlation property, which allows for a greater number of simultaneous users than the 1D CTP codes with TCK, 1D M3 sequence codes, 1D BIBD codes, and 1D BDS codes with TCK. The modified cross-correlation property removes the MUI to increase the number of simultaneous users due to photocurrent noise variance.

Figure 5 illustrates the relationship between the BER and the effective source power while keeping the data transmission rate at 2.5 Gbps and the number of simultaneous users at 48. The 1D CTP codes with TCK, 1D M3 sequence codes, 1D BIBD codes, and 1D BDS codes with TCK using the other system use photodetectors (PDs) to receive the recovered bits, resulting in the increased power consumption of the effective source power. From an effective source power = −12 dBm, the other systems based on 1D CTP codes with TCK, 1D M3 sequence codes, 1D BIBD codes, and 1D BDS codes with TCK exhibit high BER values of 10^{-9}. In contrast, the proposed system, which employs successive code weights using 1D Corite codes with TCK, shows a superior performance and requires an effective source power of −12 dBm for a BER of 10^{-9}. In contrast, the proposed 1D Corite codes with TCK require only two photodetectors at the optical receiver level due to their modified cross-correlation property, resulting in the lower power consumption of the effective source power. Figure 6 depicts the BER as a function of the data transmission rate for a given number of 48 simultaneous users and an effective source power of −12 dBm. The proposed system utilizing 1D Corite codes with TCK can achieve a higher data transmission rate of 2.5 Gbps, whereas the other systems using 1D CTP codes with TCK, 1D M3 sequence codes, 1D BIBD codes, and 1D BDS codes with TCK can reach data transmission rates of 0.6 Gbps, 0.9 Gbps, 0.4 Gbps, and 0.95 Gbps, respectively. The innovative 1D Corite codes with TCK, with their modified cross-correlation characteristics, demand just two photodetectors at the optical receiver stage, leading to a substantially higher data transmission rate. In contrast, the other systems rely on PDs to receive the recovered bits, leading to comparatively lower data transmission rates. Considering 48 simultaneous users and an effective source power of −12 dBm, a BER = 10^{-9} demonstrates the superior data transmission rate (2.5 Gbps) of the 1D Corite codes with TCK compared to the data transmission rates of 1D CTP codes with TCK, 1D M3 sequence codes, 1D BIBD codes, and 1D BDS codes with TCK.

The spectral efficiency is SE = the aggregate information rate/total spectral bandwidth = $g\,|_{\mathrm{BER}=10^{-9}} R_b/\Delta v$, where $g\,|_{\mathrm{BER}=10^{-9}}$ is the number of simultaneous user at BER = 10^{-9}, and $R_b = 1/B_r$ is the bit rate per receiver [22]. Figure 7 depicts the relationship between the code length and spectral efficiency for SAC-OCDMA systems using 1D Corite codes with TCK, 1D CTP codes with TCK, 1D M3 sequence codes, 1D BIBD codes, and 1D BDS codes with TCK. The spectral efficiency of the proposed 1D Corite codes with TCK is 0.8 with a code length of 900; that of the 1D CTP codes with TCK is 0.55 with a code length of 900; that of the 1D M3 sequence codes is 0.63 with a code length of 900; that of the 1D BIBD codes is 0.03 with a code length of 900; and that of the 1D BDS codes with TCK is 0.58 with a code length of 900. Obviously, the spectral efficiency of the proposed system using the 1D Corite codes with TCK is greater than that of the other systems using the 1D CTP codes with TCK, 1D M3 sequence codes, 1D BIBD codes, and 1D BDS codes with TCK. Therefore, the spectral efficiency of the 1D Corite codes with TCK is better than that of the other systems using 1D CTP codes with TCK, 1D M3 sequence codes, 1D BIBD codes, and 1D BDS codes with TCK.

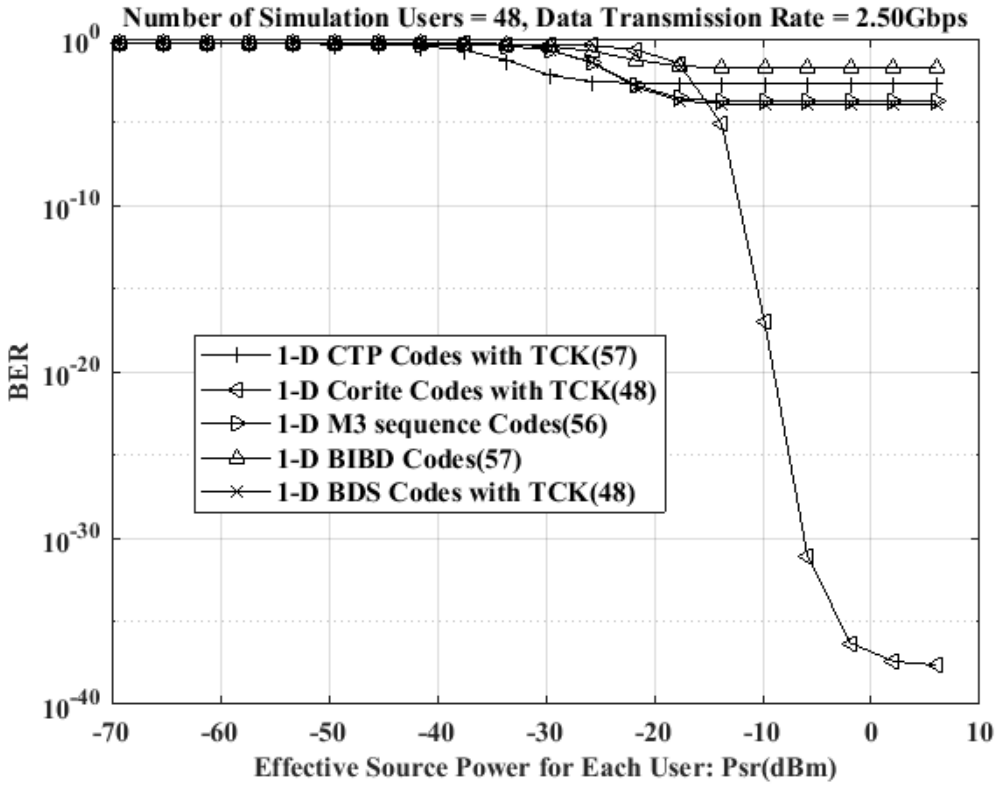

Figure 5. Comparison of BER in the proposed 1D Corite codes with TCK and other codes with different effective source powers.

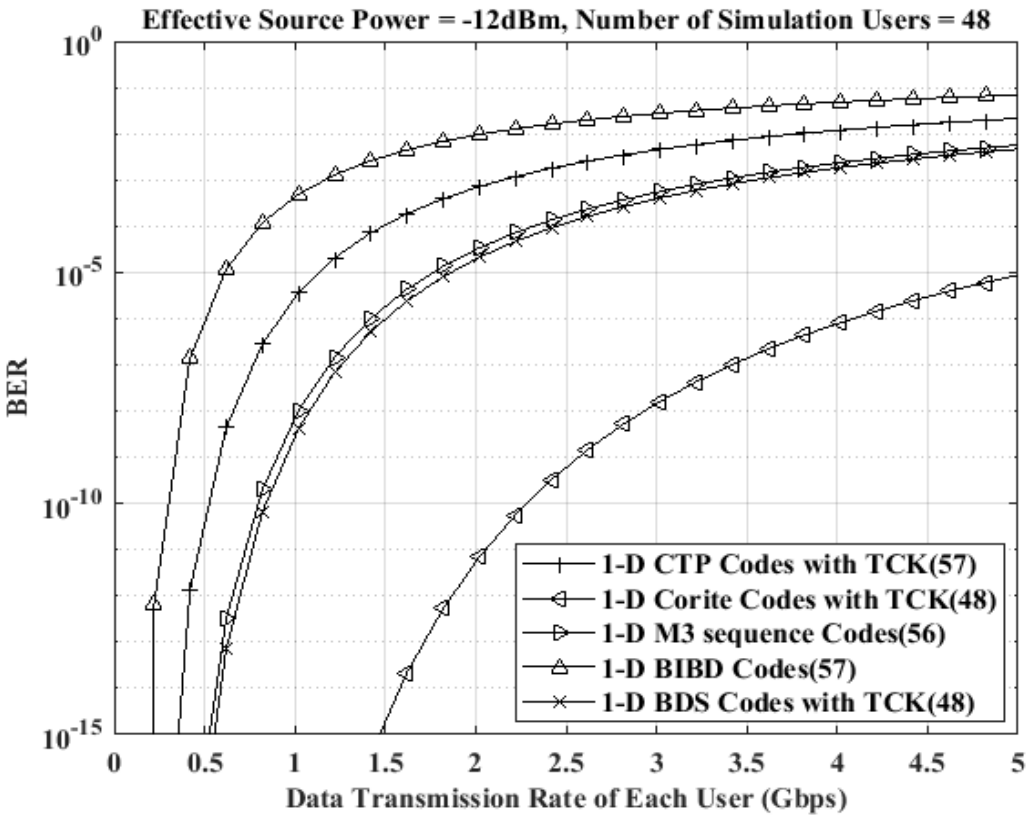

Figure 6. Comparison of BER in the proposed 1D Corite codes with TCK and other codes with different data transmission rates.

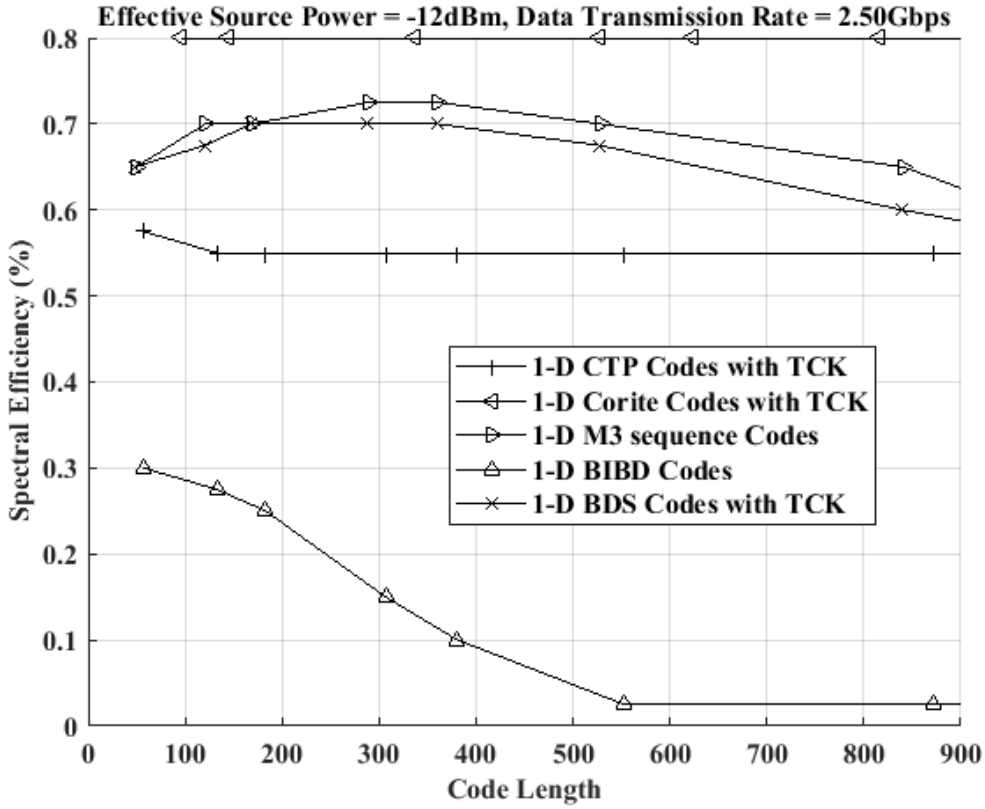

Figure 7. SE versus code length.

6. Discussion

We propose 1D Corite codes with TCK using SOPs, which are the core element of the algorithm. The cross-correlation merges the code sequences $M(\alpha)$ for 0-degree polarization and $M(\alpha')$ for 90-degree polarization. We define the values of the modified cross-correlation between $\Omega(\alpha, r)$ and $\Omega(\alpha', r')$ as $\psi(\alpha, r, \alpha', r') = \Omega(\alpha, r) - \Omega(\alpha', r')$. These values can be ξ, $-\xi$, or 0. The transmitter employs a polarizer to split the optical signal into two polarizations. Each polarization is used to operate two code sequences of the 1D Corite codes with TCK, which are then combined into a single optical signal. The receiver receives this single optical signal in both polarizations, which it separates into two distinct signals: one with 0-degree polarization and the other with 90-degree polarization. The 0-degree polarization signal is directed to the cross-correlation $\Omega(\alpha, r)$ in one photodiode, while the 90-degree polarization signal is sent to the cross-correlation $\Omega(\alpha', r')$ in a second photodiode. The modified cross-correlation is obtained by subtracting the outputs from the two photodiodes.

The transmitter uses the data from 0 bits to send the up EOM with a 1 control signal and the down EOM with a 0 control signal, creating one code sequence $M(\alpha)$ with 0-degree polarization and no optical signal with 90-degree polarization. The receiver uses a one $\times$ two PBS to separate the 0-degree polarization from the 90-degree polarization. This results in the transferal of $I_{PD0,0bit} = R\frac{P_{sr}}{\xi N}\xi$, which corresponds to the cross-correlation $\Omega(\alpha, r) = \xi$, and to $I_{PD1,0bit} = 0$, which corresponds to the cross-correlation $\Omega(\alpha', r') = 0$. The subtraction of these yields $I_{TPD,0bit} = [I_{PD0,0bit} - I_{PD1,0bit}] = R\frac{P_{sr}}{\xi N}\xi$, which corresponds to the modified cross-correlation of $\Psi(\alpha, r, \alpha', r') = \xi$. Similarly, the transmitter uses the data from 1 bit to generate no optical signal with 0-degree polarization and the code sequence $M(\alpha')$ with 90-degree polarization. The receiver then transfers to $I_{PD0,1bit} = 0$, which corresponds to the cross-correlation $\Omega(\alpha, r) = 0$, and to $I_{PD1,1bit} = R\frac{P_{sr}}{\xi N}\xi$, which corresponds to the cross-correlation $\Omega(\alpha', r') = \xi$. Subtracting these results in $I_{TPD,1bit} = [I_{PD0,1bit} - I_{PD1,1bit}] = -R\frac{P_{sr}}{\xi N}\xi$ reflects the modified cross-correlation $\Psi(\alpha, r, \alpha', r') = -\xi$.

Reference [24] used polarization to create the transmitter and receiver without utilizing TCK. The 1D CTP codes in reference [26] used TCK to create polarization by varying the code sequence content between 1 and −1, controlling the horizontal (0°) polarization with 1 and the vertical (90°) polarization with −1. Reference [27] utilized TCK to achieve TCK without polarization. The 1D Corite codes with TCK also use TCK but apply it to produce two polarizations in all code sequences for the horizontal (0°) polarization and all code sequences for the vertical (90°) polarization. Consequently, the performance of the 1D Corite codes with TCK is superior to that of references [24,26,27].

7. Conclusions

This paper presents a performance analysis of a spectral encoding SAC-OCDMA system with two mutually orthogonal SOPs based on novel 1D Corite codes with TCK. The system's BER is evaluated in terms of the SNR, taking into account the effect of the PIIN, thermal noise, and shot noise. The 1D Corite codes with TCK used in the proposed system are designed to suppress PIIN by introducing a modified cross-correlation. Compared to traditional 1D CTP codes with TCK, 1D M3 sequence codes, 1D BIBD codes, and 1D BDS codes with TCK, the proposed system using 1D Corite codes with TCK shows a superior performance. When considering a BER of 10^{-9} and a data transmission rate of 2.5 Gbps, the proposed system employing 1D Corite codes with TCK is capable of accommodating over 48 additional simultaneous users compared to the other systems employing 1D CTP codes with TCK, 1D M3 sequence codes, 1D BIBD codes, and 1D BDS codes with TCK. Specifically, with 48 simultaneous users and a data transmission rate of 2.5 Gbps, the proposed system utilizing 1D Corite codes with TCK exhibits a significantly effective source power of −12 dBm compared to the other systems employing 1D CTP codes with TCK, 1D M3 sequence codes, 1D BIBD codes, and 1D BDS codes with TCK. On the contrary, when maintaining a fixed count of 48 simultaneous users and an effective source power of −12 dBm, the data transmission rate achieved by the 1D Corite codes with TCK based the proposed system can exceed 2.5 Gbps. We will use the proposed 1D Corite codes with TCK to enhance the advanced system's architecture by utilizing SOP spectral encoding (e.g., optical medical bioenergy usage without cross-talk) in potential future research or applications.

Funding: This research received no external funding.

Institutional Review Board Statement: Not applicable.

Informed Consent Statement: Not applicable.

Data Availability Statement: All data are available in this paper.

Conflicts of Interest: The author declares no conflict of interest.

References

1. Abd, T.H.; Aljunid, S.A.; Fadhil, H.A.; Ahmad, R.B. A new algorithm for development of dynamic cyclic shift code for spectral amplitude coding optical code division multiple access systems. *Fiber Integer. Opt.* **2012**, *31*, 397–416. [CrossRef]
2. Jurado-Navas, A.; Raddo, T.R.; Garrido-Balsells, J.M.; Borges, B.-H.-V.; Olmos, J.J.V.; Monroy, I.T. Hybrid optical CDMA-FSO communications network under spatially correlated gamma-gamma scintillation. *Opt. Exp.* **2016**, *24*, 16799. [CrossRef] [PubMed]
3. Raddo, T.R.; Sanches, A.L.; Tafur Monroy, I.; Borges, B.V. Throughput performance evaluation of multiservice multirate OCDMA in flexible networks. *IEEE Photon. J.* **2016**, *8*, 1–15.
4. Sanches, A.L.; Raddo, T.R.; dos Reis, J.V.; Borges, B.-H.V. Performance analysis of single and multirate FFH-OCDMA networks based on PSK modulation formats. *J. Opt. Commun. Netw.* **2015**, *7*, 1084–1097. [CrossRef]
5. Mostafa, S.; Mohamed, A.E.-N.A.; El-Samie, F.E.A.; Rashed, A.N.Z. Performance evaluation of SAC-OCDMA system in free space optics and optical fiber system based on different types of codes. *Wirel. Pers. Commun.* **2017**, *96*, 2843–2861. [CrossRef]
6. Hacini, L.; Aissaoui, A. A novel mapping technique for an adaptive length of codes in SAC-OCDMA systems. *Wirel. Pers. Commun.* **2022**, *123*, 1103–1119. [CrossRef]
7. Mrabet, H.; Cherifi, A.; Raddo, T.; Dayoub, I.; Haxha, S. A Comparative Study of Asynchronous and Synchronous OCDMA Systems. *IEEE Syst. J.* **2020**, *15*, 3642–3653.

8. Chaudhary, S.; Sharma, A.; Tang, X.; Wei, X.; Sood, P. A cost effective 100 Gbps FSO system under the impact of fog by incorporating OCDMAPDM scheme. *Wirel. Pers. Commun.* **2021**, *116*, 2159–2168. [CrossRef]
9. dos Reis, J.V., Jr.; Raddo, T.R.; Sanches, A.L.; Borges, B.V. Fuzzy logic control for the mitigation of environmental temperature variations in OCDMA networks. *J. Opt. Commun. Netw.* **2015**, *7*, 480–488. [CrossRef]
10. Kumari, M.; Arya, V. Investigation of high-speed hybrid WDM-OCDMA-PON system incorporating integrated fiber-FSO link under distinct climate conditions. *Opt. Quantum Electron.* **2022**, *54*, 775–804. [CrossRef]
11. Alayedi, M.; Cherifi, A.; Hamida, A.F.; Mrabet, H. A fair comparison of SAC-OCDMA system configurations based on two dimensional cyclic shift code and spectral direct detection. *Telecommun. Syst.* **2022**, *79*, 193–212. [CrossRef]
12. Singh, M.; Aly, M.H.; Abd El-Mottaleb, S.A. Performance analysis of 6 × 10 Gbps PDM-SAC-OCDMA-based FSO transmission using EDW codes with SPD detection. *Optik* **2022**, *264*, 169415–169426. [CrossRef]
13. Singh, M.; Atieh, A.; Aly, M.H.; El-Mottaleb, S.A.A. 120 Gbps SAC-OCDMA-OAM-based FSO transmission system: Performance evaluation under different weather conditions. *Alex. Eng. J.* **2022**, *61*, 10407–10418. [CrossRef]
14. Nisar, K.S.; Ahmed, H.Y.; Zeghid, M.; Imtiaz, W.A.; Sarangal, H.; Thapar, S.S. The multi-service schemes for SAC-OCDMA systems with variable code weight. *Opt. Quantum Electron.* **2021**, *53*, 293–310. [CrossRef]
15. Abd El-Mottaleb, S.A.; Fayed, H.A.; Ismail, N.E.; Aly, M.H.; Rizk, M.R.M. MDW and EDW/DDW codes with AND subtraction/single photodiode detection for high performance hybrid SAC-OCDMA/OFDM system. *Opt. Quantum Electron.* **2020**, *52*, 239–259. [CrossRef]
16. Sarangal, H.; Thapar, S.S.; Nisar, K.S.; Singh, M.; Malhotra, J. Performance estimation of 100 GB/s hybrid SACOCDMA–FSO-MDM system under atmospheric turbulences. *Opt. Quantum Electron.* **2021**, *53*, 598–611. [CrossRef]
17. Aissaoui, A.; Hacini, L. Enhancing UWOC link performance using a hybrid OFDM/SAC-OCDMA system. *Opt. Quantum Electron.* **2024**, *56*, 28–45. [CrossRef]
18. Abd El-Mottaleb, S.A.; Fayed, H.; Abd El-Aziz, A.; Metawee, M.; Aly, M.H. Enhanced spectral amplitude coding OCDMA system utilizing a single photodiode detection. *Appl. Sci.* **2018**, *8*, 1861. [CrossRef]
19. Sasaki, K.; Minato, N.; Ushikubo, T.; Arimoto, Y. First OCDMA experimental demonstration over free space and optical fiber link. In Proceedings of the OFC/NFOEC Conference on Optical Fiber Communication/National Fiber Optic Engineers Conference, San Diego, CA USA, 24–28 February 2008; pp. 1–3.
20. Moghaddasi, M.; Seyedzadeh, S.; Glesk, I.; Lakshminarayana, G.; Anas, S.B.A. DW–ZCC code based on SAC-OCDMA deploying multi-wavelength laser source for wireless optical networks. *Opt. Quantum Electron.* **2017**, *49*, 393–406. [CrossRef]
21. Galdino, L.; Raddo, T.R.; Sanches, A.L.; Bonani, L.H.; Moschim, E. Performance comparison of hybrid 1-D WDM/OCDMA and 2-D OCDMA towards future access network migration scenario. In Proceedings of the 14th International Conference on Transparent Optical Networks (ICTON), Coventry, UK, 2–5 July 2012; pp. 1–4.
22. Chang, T.W.F.; Sargent, E.H. Optimizing spectral efficiency in multiwavelength optical CDMA system. *IEEE Trans. Commun.* **2003**, *51*, 1442–1445. [CrossRef]
23. He, C.; Xiao, S.; Yi, L.; Zhou, Z.; Zhu, M.; Shi, J.; Dong, Y.; Hu, W. A tunable encoder/decoder based on polarization modulation for the SAC-OCDMA PON. *IEEE Photonics Technol. Lett.* **2011**, *23*, 748–750.
24. Tarhuni, N.G. Investigation of multi-beam interference impact on state-of-polarization OCDMA optical networks. In Proceedings of the 2019 International Symposium on Networks, Computers and Communications (ISNCC), Istanbul, Türkiye, 18–20 June 2019; pp. 1–6.
25. Heritage, J.P.; Weiner, A.M. Advances in Spectral Optical Code-Division Multiple-Access Communications. *IEEE J. Sel. Top. Quantum Electron.* **2007**, *13*, 1351–1369. [CrossRef]
26. Tseng, S.-P. A new polarization-SAC scheme suitable for compact OCDMA-FSO networks. *IEEE Syst. J.* **2018**, *13*, 1332–1335. [CrossRef]
27. Yang, C.-C. Spectral efficiencies of the optical CDMA-based PONs using two-code keying. *IEEE Commun. Lett.* **2010**, *14*, 767–769. [CrossRef]
28. Wei, Z.; Hooshang, G.-S. Codes for spectral-amplitude-coding optical CDMA systems. *J. Light. Technol.* **2002**, *20*, 1284–1291.
29. Yang, C.-C. Spectral Amplitude Coding Optical CDMA Networks Using 2m × 2m Waveguide Gratings. *IEEE Photonics Technol. Lett.* **2010**, *22*, 1835–1837. [CrossRef]